Novel LC Composition for Improved Performance in Millimeter-Wave Reflectarrays

Dayan Pérez-Quintana[(1)], Jose A. Marcotegui[(2)], Sergei A. Kuznetsov[(3)], Valeri I. Lapanik[(4)], Miguel Beruete[(5),(6)]
dayan.perez@unisi.it, jmarcotegui@tafcomw.com, sakuznetsov@nsu.ru, lapanik@yahoo.com, miguel.beruete@unavarra.es
[(1)]Department of Information Engineering and Mathematics, University of Siena, Italy
[(2)]TAFCO Metawireless, Navarra, Spain
[(3)]Novosibirsk State University, Novosibirsk, Russia.
[(4)]Institute of Applied Physical Problems, Minsk, Belarus.
[(5)]Department of Electrical, Electronic and Communications Engineering, Universidad Pública de Navarra, Spain.
[(6)]Institute of Smart Cities (ISC), Universidad Pública de Navarra, Spain.

***Abstract*—A reconfigurable liquid crystal (LC) based reflectarray (RA) designed for operation in the D-band from 105 to 125 GHz is numerically demonstrated. The device has a configuration of a high-impedance surface with a meta-array of 29×33 patches on a 2-mm-thick quartz substrate separated from the ground plane through a 40 μm-thick LC layer. The electric biasing of the LC-loaded RA unit cells is realized by introducing narrow inductive strips connecting neighboring patches in one dimension. A novel LC composition with low dielectric losses ($<$ 0.003) and high dielectric anisotropy ($>$ 1.3) has been developed for operation at millimeter-waves. The results demonstrate a reflection phase tunability of 210° and low insertion losses of 2.5 dB. Furthermore, the device was demonstrated as a proof of concept for 1D beam-steering applications, exhibiting an operational bandwidth of 12 GHz.**

I. Introduction

Reconfigurable or tunable array antennas have attracted a significant interest in the last years due to their advantages over conventional phased arrays such as adaptability, versatility, spectrum efficiency, reduced size and weight, cost-effectiveness, and interference mitigation [1]. Active devices have been an interesting option to modify the radiation properties of designs operating at millimeter-waves (mmWaves) incorporating active elements like PIN and MEMS [2]–[4]. Nevertheless, the difficulty in manufacturing, the losses, and the parasitic effects on these devices at sub-millimetre waves discourage their use in frequency bands above 50 GHz [5]. Additionally, complex networks are required to feed these devices and integrate them in the final structure, taking care not to disturb the radiation performance and assuring compactness. Moreover, the bandwidth limitations due to the possible interactions of the fields with the feeding network or just for the operation band of the active element can hinder a satisfactory final result.

Liquid crystals (LC) are a promising alternative in the technology of electronically reconfigurable/switchable reflectarrays (RA) operating in the mmWaves and terahertz band. LC is a particular aggregate state of matter which has characteristics of both solids and liquids [6], [7]. Two essential characteristics of LC molecules are that they are uniaxial and can be rotated/aligned by applying an external biasing voltage (amongst other techniques), allowing for tuning of the effective dielectric permittivity. Since their introduction, the main applications of LCs have been related to high-resolution displays and spatial light modulators operating at optical frequencies [8]. It is worth highlighting that a fundamental obstacle to translate LC based tunable devices to lower frequencies such as microwaves and mmWaves is the stark contrast between the LC-layer thickness (typically 2-10 μm) compared to the wavelength (in the centimeter and millimeter-scale). When the radiation propagates perpendicular to the LC layer, this results in weak wave-LC interaction, leading to the negligible tuning of the response when the LC is modulated. Moreover, the values of the LC permittivity along the ordinary and extraordinary axes are not drastically different; hence, a large LC thickness is necessary to obtain significant phase differences at the output. However, a large thickness of the

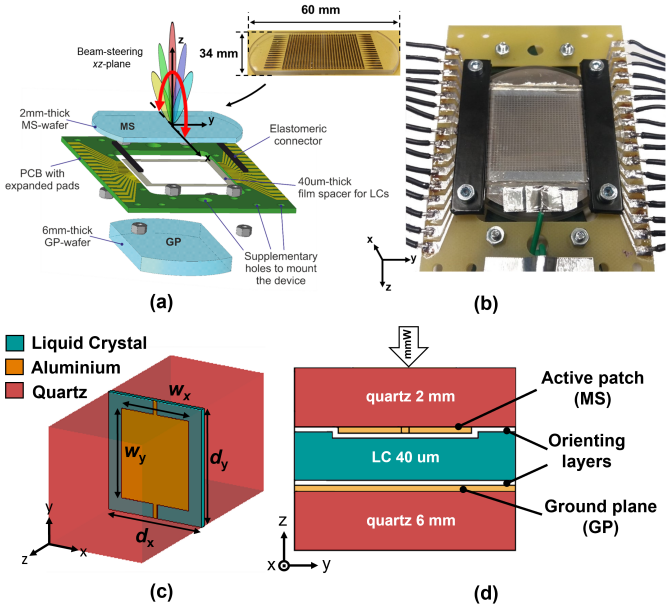

Fig. 1. Schematic representation of the manufactured RA: (a) Isometric exploded view of all the pieces composing the RA and showing in the center the PCB used to realize the bias connection. Inset, front view of the 2-mm-thick quartz wafer with active patches (MS) and contact pads, which has a size of 34 mm by 60 mm. . (b) Photo of the assembled device prepared for connection to a 33-channel voltage generator. LC-based RA unit cell: (c) isometric view with the main dimensions; (d) cross-sectional view, showing the materials and arrangement.

LC would imply high external voltages to bias it properly, resulting in damage of the LC due to dielectric breakdown.

To overcome these limitations, resonant structures can be devised to obtain LC-based tunable devices at microwaves and mmWaves [5], [9]. The underlying mechanism is based on the property that the phase (for the moment, it could be in transmission or reflection) near a resonance undergoes a fast variation, leading to a steep slope in the frequency response. Intuitively, this fast variation can be interpreted as if the structure was made effectively larger. Hence, in the vicinity of the resonance, modulation of the LC permittivity by rotating the LC molecules from the ordinary to the extraordinary axis or vice versa can lead to a significant phase difference at the output. In [10], LC unit cells operating in the X-band were analyzed. A tunable dynamic phase range of 221° was achieved over a band of 220 MHz (fractional bandwidth of 2.2%) using a K15 nematic LC. A similar strategy was exploited in [11], where a printed RA antenna was simulated and manufactured in the X-band. There, a reconfigurable monopulse-shaped radiation pattern was demonstrated using a metallic microstrip patch sitting on a 500 μm cavity filled with a LC substrate by dynamically switching the permittivity of the LC substrate in the two halves of a RA aperture. In [12], a RA consisting of 52×54 identical cells composed of three parallel dipoles of different lengths placed on an LC substrate and operating in the F-band was proposed. This design exhibited an 8% fractional bandwidth with moderate losses (∼7 dB), using a low-cost manufacturing process to produce antennas in frequencies from 60 to 500 GHz.

In this work, a reconfigurable RA with low losses and moderate bandwidth is implemented using a novel nematic LC composition [13], see Fig. 1(a) and (b). With an LC thickness of 40 μm, this resonant structure was designed to operate in the frequency band of 105-120 GHz. Hence, our experimental results underscore the ground-breaking capabilities of LC technology in the millimeter wave domain. We have successfully achieved precise beam guidance in the intended direction by utilizing an LC-based reconfigurable reflectarray. A pivotal aspect of this research was the development of a unique LC composition tailored exclusively for millimeter-wave applications. Our device demonstrates exceptional performance, with impressively low loss values of approximately 2.5 dB. This novel LC composition requires further testing and optimization to exploit its capabilities fully. Nonetheless, this investigation provides compelling evidence of LC immense technological potential in reconfigurable devices operating at mmWaves.

II. DESIGN, NUMERICAL AND EXPERIMENTAL RESULTS

The unit cell of the proposed RA has a width $d_x = 0.9\,\mathrm{mm}$ and a height $d_y = 1.05\,\mathrm{mm}$, as depicted in Fig. 1(c). The structure consists of two quartz wafers, of thickness 2 and 6 mm respectively, represented in red. Quartz was selected due to its low dielectric losses in the frequency range of interest, as discussed below. The LC material, depicted in cyan, is deposited between both wafers and has a height of 40 μm ($h_{LC} = 40\,\mu\mathrm{m}$). The metasurface (MS) is patterned on the bottom surface of the $2\,\mathrm{mm}$ quartz wafer, laying over the

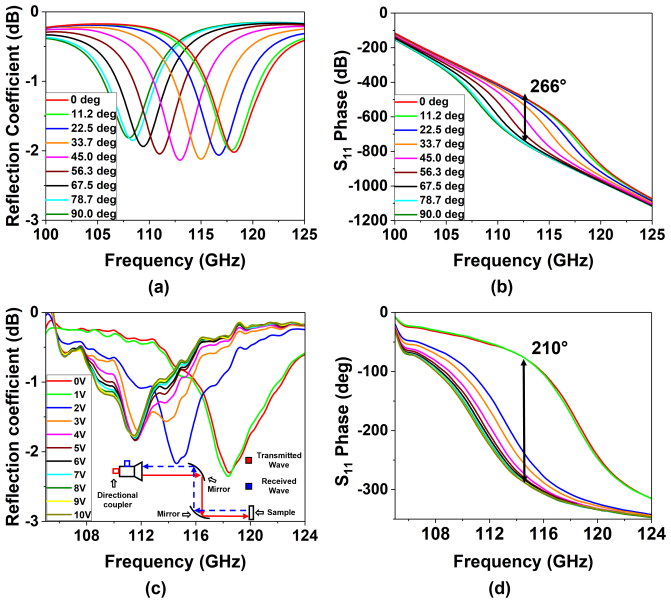

Fig. 2. Simulated and measured characteristics of the RA for different orientation angles of the LC director and a biasing voltage variation from 0 V to 10 V, respectively. Simulation results: (a) reflection coefficient magnitude in dB; (b) reflection phase in degrees. Measurement results: (c) reflection coefficient magnitude in dB; (d) reflection phase in degrees.

LC substrate. The MS unit cell consists of a rectangular aluminum patch with transverse dimensions $w_x = 0.65\,\mathrm{mm}$ and $w_y = 0.08\,\mathrm{mm}$ and thickness $t = 0.4\,\mu\mathrm{m}$ connected through narrow strips $70\,\mu$m-wide to the vertically neighboring unit cells (represented in orange), which serve to distribute the same electric potential to all patches for LC biasing. The lower electrode is composed of a uniform, $0.4\,\mu$m-thick aluminum layer, serving as the ground plane (GP) bottom electrode, and held at a zero potential. As shown in Fig. 1(b), two thin orienting layers are deposited onto both the MS and GP. They are made of poly(vinyl alcohol) and have a subwavelength thickness ($\leq 0.1\,\mu\mathrm{m}$) so they have negligible impact on the electromagnetic response of the device. These orienting layers are crucial in LC technology as they ensure proper alignment of the LC molecules through a mechanical rubbing process. The LC molecules are aligned parallel to the y-axis in the present design when no bias voltage is applied.

All the full-wave simulations in this work were performed using the commercial electromagnetic software CST Microwave Studio® [14]. Aluminum was modeled as a lossy metal with conductivity σ = 3.56 × 10^7 S/m, and quartz as a dielectric with a complex relative permittivity $\varepsilon_{Quartz} = 3.78(1 - j0.002)$. The inherently anisotropic LC medium was modeled using a complex dielectric permittivity tensor $\bar{\bar{\epsilon}}$. In general, the local components of $\bar{\bar{\epsilon}}$ at every point of the LC layer depend on the orientation of the local director vector of LC molecules. This vector is the local optical axis of each LC molecule and is a function of the local bias electric field inside the medium [13].

Fig. 2(a) and (b) show the amplitude and the phase of the reflection coefficient for an angular variation on the orientation of the local director vector from 0 to 90°. As shown in Fig. 2(a), there is a resonant dip in the spectrum of the reflection coefficient magnitude which shifts from 117 to 108 GHz when

the LC tensor is rotated from 0° to 90°. In all considered cases, its magnitude is above −2.5 dB within the entire frequency band. This resonance is accompanied by a phase variation [Fig. 2(b)] which can be modulated by rotating the LC tensor. A maximum phase excursion of 266° is obtained at 113 GHz. There, it can be appreciated clearly the range of phases achieved by rotating the permittivity tensor. These results provide a complete characterization of the reflection phase as a function of the orientation of the local director vector and confirm the necessity of working in the vicinity of a resonance to observe a significant phase excursion.

To corroborate experimentally the previous results, the designed RA prototype was fabricated and measured. The prototype contains 29×33 unit cells with overall dimensions of 29.7×30.45 mm. Fig. 1(a) and (b) provides a detailed illustration of the biasing configuration used in the prototype. The 33 columns are connected to corresponding metallic pads to introduce the biasing voltage, enabling proper LC operation [13]. Contact photolithography was used to create the MS pattern on the $2\,\mathrm{mm}$-thick quartz wafer, which included the active patch array and elongated contact pads for electric connection to individual biasing lines. To avoid narrow gaps between the pads, they were separated into two sets: 17 pads were placed on one side to control the odd biasing lines, while 16 pads were located on the opposite side to govern the even ones, as shown in Fig. 1(a) and (b).

A Vector Network Analyzer (MVNA-8-350, AB Millimetre) was used to characterize the fabricated RA. The samples were measured in the frequency range of 105-125 GHz with a step of 50 MHz. A horn antenna was used to transmit the wave, which was then focused on the sample by a pair of elliptical mirrors (see inset in Fig. 2(c)). In the first set of experiments, all biasing lines were driven at the same voltage, so the reflected wave traveled in the normal direction (since there was no phase difference among the unit cells). The reflected wave was then detected by the horn antenna, guided by the elliptical mirrors, and steered to the detector through a directional coupler connected to the antenna. Before the characterization, the setup was calibrated by placing a mirror in the sample position. The biasing voltage was varied from 0 V to 10 V in increments of 0.50 V, but for clarity, the curves are presented with a step of 1 V.

Fig. 2(c) presents the measured reflection coefficient magnitude. The losses obtained in the measurements are comparable to those obtained in the simulation [Fig. 2(a)], with a minimum reflection coefficient around 2.5 dB. A shift in frequency towards higher frequencies with respect to simulation results was observed, especially near the maximum bias state. The maximum experimental phase deviation was 210°, which is 56° lower than the simulation results, as seen in Fig. 2(d). There is also an abrupt change in phase between 1 V (light green curve) and 2 V (dark blue curve), indicating that the LC molecules have maximal sensitivity in this region, and a small variation in biasing voltage yields substantial changes in LC director orientation. Despite these differences, the experimental results validate the simulation, the good performance of the LC, and the correct bias connection implemented in the prototype. These results give a complete characterization of the reflection phase with a uniform bias voltage.

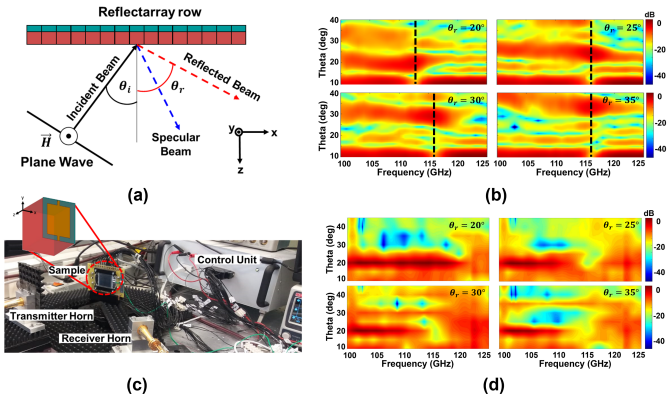

Fig. 3. (a) Beam-steerer simulation scenario where $\theta_i = 10$ deg is the angle of the incident beam and θ_r is the angle of the beam reflected in the desired direction. (b) Contour plot diagram for a beam reflected at: 20°, 25°, 30° and 35°. (c) Photograph of the measurement scenario composed of two horn antennas and a rotating positioner where the RA under test is placed. (d) Contour plot diagram for the same reflected beams. Scale is in dB and each panel is normalized to the maximum.

A beam steerer that operates in reflection can be designed by incorporating a phase variation into the metasurface, as described by the following equation:

$$\phi(n) = k_0 dn \left(\sin(\theta_r) - \sin(\theta_i)\right) \tag{1}$$

where n is an integer that labels each column in the array, θ_r is the desired reflection angle, θ_i is the angle of incidence, $\phi(x)$ is the phase of each column composing the RA, achieved by rotating the local director vector. Note that a modulation of the RA phase can only be achieved along the x axis since the columns are electrically connected and share the same biasing voltage.

For the numerical analysis, a single row consisting of 1×33 unit cells was considered, with periodic boundary conditions applied along the y-direction (infinite in that direction) and open boundary conditions with an additional space (open+add space) along the x- and z-directions, as depicted in Fig. 3(a). The structure was illuminated by a plane wave with H_y transversal electric (TM) polarization with an incidence angle of $\theta_i = 10$ deg.

Fig. 3(b) present contour plot diagrams representing the radar cross section far-field patterns as a function of frequency and angle when the RA is configured to produce a reflected beam at 20°, 25°, 30°, and 35°, respectively. As shown in the contour plot diagram, in all cases the main reflection beam occurs at 10° (that corresponds to the specular reflection) in all the considered bandwidth except at the operation band wherein the RA is able to deflect the beam towards the desired direction (as indicated by the dashed lines). To validate the simulation results, a second set of experiments is proposed [Fig. 3(c)], where a non-uniform biasing was applied to the RA.

The experimental setup consisted of two horn antennas (working in D-band from 105 to 125 GHz) and a sample holder where the RA was placed. The sample holder was positioned on a rotary platform to control the angle of incidence and the receiving antenna was placed on a platform connected to the rotary platform to freely rotate and scan the angular power distribution. The experimental setup was

covered with absorbing resin to minimize ambient reflections and a 33-channel voltage generator was used to independently feed all the biasing lines of the RA. All the setup implemented for this second experiment is illustrated in Fig. 3(c). To further characterize the beam steering performance of the device, the incidence angle between the transmitter and the RA was fixed at 10 degrees. The biasing of the RA unit cells was properly controlled by adjusting the voltage generator to achieve the desired angle of reflection. In this case, the measurement was focused on analyzing the transmission coefficient using the secondary horn antenna positioned at the reception location. The transmission coefficient peak should correspond to the analyzed output direction in simulations. As was done in the simulation analysis, Fig. 3(d) shows a contour plot study of the transmission coefficient for different frequencies when the RA is configured to get a beam at 20°, 25°, 30° and 35°. The presence of the specular beam at θ =10° is clearly evident and significantly influences the quality of the beam at lower beam-steered angles.

Beyond that, analysis of Fig. 3(d), specifically to $\theta_r = 20°$, reveals that the device exhibits good pointing performance over a wide bandwidth, from 105 to 120 GHz, thus validating the correct biasing and confirming the results of the simulation. However, at $\theta_r = 25°$, the bandwidth is reduced compared to the previous result, and the beam resolution is not as high. Nevertheless, the outcomes for the other angles demonstrate good behavior, displaying adequate beam pointing in the intended direction and retaining a sufficient bandwidth, which in most cases extends from 105 to 120 GHz.

III. Conclusion

This research introduces a reconfigurable LC-loaded reflectarray, engineered to operate close to 110 GHz. The reflectarray comprises a high-impedance surface with a patch meta-array arranged on a quartz substrate, which is 2-mm thick, separated from the ground plane by a 40-μm LC layer. To electrically bias the LC-loaded unit cells, narrow inductive strips connecting adjacent patches in one dimension were added. Simulations reveal a maximum phase shift of 266° with losses below 3 dB. In a 1D beam steering scenario, when appropriately tuned, the reflected beam aligns with the desired direction at the operational frequency. The fabricated prototype, consisting of 29×33 unit cells, demonstrates a maximum phase shift of 210° with losses of approximately 2.5 dB. Experimental findings confirm the device's ability to steer the beam accurately within a bandwidth of approximately 12 GHz. These outcomes underscore the potential of LC technology for reconfigurable devices operating in millimeter and submillimeter wave ranges, offering straightforward solutions for emerging applications.

Acknowledgements

This work was supported by Project PID2022-137845NB-C21 funded by MICIU/AEI /10.13039/501100011033 and by FEDER, UE; S.A.K. acknowledges support from the Ministry of Science and Higher Education of the Russian Federation, grant 075-15-2020-797 (13.1902.21.0024). The authors also thank the Shared Equipment Center "Spectroscopy and Optics" of the Institute of Automation and Electrometry SB RAS for THz-TDS characterization of quartz wafers.

References

[1] S. V. Hum and J. Perruisseau-Carrier, "Reconfigurable reflectarrays and array lenses for dynamic antenna beam control: A review," *IEEE Transactions on Antennas and Propagation*, vol. 62, no. 1, pp. 183–198, 2014.

[2] H. Zhang, X. Chen, Z. Wang, Y. Ge, and J. Pu, "A 1-Bit Electronically Reconfigurable Reflectarray Antenna in X Band," *IEEE Access*, vol. 7, pp. 66567–66575, 2019.

[3] Chih-Chieh Cheng and A. Abbaspour-Tamijani, "Evaluation of a Novel Topology for MEMS Programmable Reflectarray Antennas," *IEEE Transactions on Microwave Theory and Techniques*, vol. 57, pp. 3333–3344, dec 2009.

[4] O. Bayraktar, O. A. Civi, and T. Akin, "Beam switching reflectarray monolithically integrated with RF MEMS switches," *IEEE Transactions on Antennas and Propagation*, vol. 60, no. 2 PART 2, pp. 854–862, 2012.

[5] G. Perez-Palomino, J. Encinar, M. Barba, and E. Carrasco, "Design and evaluation of multi-resonant unit cells based on liquid crystals for reconfigurable reflectarrays," *IET Microwaves, Antennas & Propagation*, vol. 6, no. 3, p. 348, 2012.

[6] S. C. Pavone, E. Martini, F. Caminita, M. Albani, and S. Maci, "Surface Wave Dispersion for a Tunable Grounded Liquid Crystal Substrate Without and With Metasurface on Top," *IEEE Transactions on Antennas and Propagation*, vol. 65, pp. 3540–3548, jul 2017.

[7] E. Martini, S. C. Pavone, M. Albani, S. MacI, V. Martorelli, G. Giodanengo, A. Ferraro, R. Beccherelli, G. Toso, and G. Vecchi, "Reconfigurable antenna based on liquid crystals for continuous beam scanning with a single control," *2019 IEEE International Symposium on Antennas and Propagation and USNC-URSI Radio Science Meeting, APSURSI 2019 - Proceedings*, no. 4000114502, pp. 449–450, 2019.

[8] M. Sharma, N. Hendler, and T. Ellenbogen, "Electrically Switchable Color Tags Based on Active Liquid-Crystal Plasmonic Metasurface Platform," *Advanced Optical Materials*, vol. 8, p. 1901182, apr 2020.

[9] J. Wu, Z. Shen, S. Ge, B. Chen, Z. Shen, T. Wang, C. Zhang, W. Hu, K. Fan, W. Padilla, Y. Lu, B. Jin, J. Chen, and P. Wu, "Liquid crystal programmable metasurface for terahertz beam steering," *Applied Physics Letters*, vol. 116, 3 2020.

[10] K. Lu, "Spatial Phase Modulator," *Optical Engineering*, vol. 29, no. 3, pp. 240–246, 1990.

[11] R. Stevenson, M. Sazegar, A. Bily, M. Johnson, and N. Kundtz, "Metamaterial surface antenna technology: Commercialization through diffractive metamaterials and liquid crystal display manufacturing," *2016 10th International Congress on Advanced Electromagnetic Materials in Microwaves and Optics, METAMATERIALS 2016*, no. September, pp. 349–351, 2016.

[12] W. Hu, R. Dickie, R. Cahill, H. Gamble, Y. Ismail, V. Fusco, D. Linton, N. Grant, and S. Rea, "Liquid Crystal Tunable mm Wave Frequency Selective Surface," *IEEE Microwave and Wireless Components Letters*, vol. 17, pp. 667–669, sep 2007.

[13] D. Pérez-Quintana, E. Aguirre, E. Olariaga, S. A. Kuznetsov, V. I. Lapanik, V. S. Sutormin, V. Y. Zyryanov, J. A. Marcotegui, and M. Beruete, "Reconfigurable millimeter-wave reflectarray based on low-loss liquid crystals," *IEEE Transactions on Antennas and Propagation*, vol. 72, no. 1, pp. 531–541, 2024.

[14] (2023). CST STUDIO SUITE.®, "[Online]. Available: https://www.3ds.com/ products-services/simulia/products/cst-studio-suite."